Department of Veterans Affairs

Journal of Rehabilitation Research and Development
Vol. 40, No. 2, March/April 2003
Pages 131–146

# Failure analysis of composite femoral components for hip arthroplasty

**Chaodi Li, PhD; Christopher Granger, MS; H. Del Schutte Jr., MD; Sherrill B. Biggers Jr., PhD; John M. Kennedy, PhD; Robert A. Latour Jr., PhD**

*Department of Bioengineering and Department of Mechanical Engineering, Clemson University, Clemson, SC; Department of Orthopedic Surgery, Medical University of South Carolina, Charleston, SC*

**Abstract—**In this research, a numerical method was developed for predicting the progressive failure of thick laminated composite femoral components. A three-dimensional (3-D) global/3-D local technique was developed to capture the overall structural response of this system, while also enabling the 3-D ply-level stress state to be determined efficiently and accurately. Different failure criteria and material degradation models were incorporated in the method, giving it the flexibility to model a wide range of materials and structures. Numerical modeling was also conducted to design experimental test methods to simulate in vivo loading conditions for component fatigue tests. Parametric studies were then conducted with the numerical model of the experimental system. Next, we compared the results to the damage behavior of the experimentally determined laminated composite femoral component to assess which parameter set most accurately predicted the actual damage development behavior. We then applied the best-fitting parameter set to analyze simulated in situ composite femoral components. Results showed that this methodology efficiently and accurately predicted damage initiation and propagation. This research demonstrates how analytical and numerical models may be used before conducting extensive experimental tests as initial tools to evaluate components for the design of composite hip implants that possess a high level of damage resistance and damage tolerance.

**Key words:** composite, failure, finite element, hip replacement, prosthesis.

## INTRODUCTION

Over an estimated 800,000 total hip replacements are being performed worldwide annually [1]. A potential cause of failure of the femoral stems is bone loss in the proximal femoral cortex following hip replacement [1–6]. Also, revision arthroplasty can be greatly complicated by an excessive loss of bone stock [4–9]. The potential for maintaining better bone stock provides the primary rationale and sparked the initial interest in exploring composite materials for hip prosthesis applications [4–6]. Hip prostheses made from composites have been evaluated by experimental testing, finite element (FE) analysis, and animal trials [4–27]. Several experiments have been performed to simulate the responses of the composite materials in hip prosthesis systems, including the effects of creep,

**Abbreviations:** CPU = central processing unit, CT = computerized tomography, FE = finite element, FRP = fiber reinforced polymer, NIH = National Institutes of Health, SED = strain energy density, SRC = stiffness reduction coefficient, THA = total hip arthroplasty.

**This material was based on work supported by the Department of Veterans Affairs, Veterans Health Administration, Rehabilitation Research and Development Service, Ralph H. Johnson Medical Center, Charleston, South Carolina.**

Address all correspondence and requests for reprints to Prof. Robert A. Latour Jr., Department of Bioengineering, 501 Rhodes Hall, Clemson University, Clemson, SC 29634; 864-656-3051; fax: 864-656-4466; email: rlatour@ces.clemson.edu.

DOI: 10.1682/JRRD.2003.03.0133

moisture, impact, and fatigue loading [4,6,13–21]. Advanced composites appear to be promising for implant applications because of their high degree of biocompatibility and good tailorability regarding strength and stiffness [4–7]. Results of experimental and modeling studies showed that stress shielding was lower for a composite prosthesis compared to metallic (titanium, cobalt-chromium) prostheses [7,15–25]. Animal models of total hip replacement have shown that cortical bone loss is reduced following the use of reduced stiffness stems [10]. Animal studies have also demonstrated that the use of composite stems can enhance proximal bony ingrowth, increase proximal medullary bone density, and prevent distal hypertrophy [5,10–12].

One aspect, which is often overlooked, is that higher interface shear stresses in the proximal region between the implant and the bone may increase with the decreasing stiffness of the implant [3,6,16,28]. Excessive shear stresses can lead to mechanical instability and thus are potential initiating mechanisms of implant loosening through the failure of supporting tissue and/or the generation of debris [7]. Research has demonstrated that the interface shear stresses are lower in the distal region for the lower modulus composite prosthesis than for a metallic prosthesis [7,17]. Although the interface shear stresses were increased in the proximal region, this may be an acceptable trade-off, since the shear stresses in the distal region generally were much higher than those in the proximal region [7]. Studies have shown that the composite hip stem compared quite well with conventional metallic hip stems in consideration of axial migration and stem subsidence [12]. Research has also shown that with appropriate stem design and insertion technique, good initial stability can be obtained with a composite hip stem [12]. If the responses are similar in humans, these findings could provide support for the development of composite materials for hip prosthesis applications. However, the transfer of load more proximally in the femur as provided by femoral component designs with low flexural stiffness will inherently lead to more challenging problems related to femoral component fixation and wear debris generation compared to higher stiffness stems. Obviously, these issues are extremely important and must be satisfactorily resolved before any low stiffness femoral component designs for hip joint replacement are considered.

Another aspect, which has not been addressed adequately, is the strength and durability of composite prosthesis stems in hip replacement applications. Research has pointed out that higher strains are generated inside the flexible implants compared with those inside stiffer devices at equal loads [16]. Implants that are more flexible thus require superior fatigue properties to avoid stem fatigue fractures [16]. Fatigue failure of composite hip stems has been shown experimentally and in clinical trials as well [5,14,21]. Thus, hip stem fatigue strength is a serious concern. To prevent such early failures in the future, improving the ability to predict composite component damage behavior and using this ability to improve damage resistance through better implant design are necessary. However, failure analysis of laminated fiber reinforced polymer (FRP) composites in total hip arthroplasty (THA) applications presents a highly complex multiscale structural design problem [13,17,24,25]. In FE analysis, either geometric approximations (two-dimensional [2-D], axi-symmetric, three-dimensional [3-D] but not anatomic) and/or material approximations (isotropic or in-plane properties only) are usually made to make the models tractable with respect to central processing unit (CPU) time, computer memory, and the storage space required. Before this present study, an efficient and accurate damage analysis methodology did not exist to enable and augment the investigation of damage behavior in composite femoral components.

For this problem to be addressed, an FE numerical method was developed to predict the progressive failure of a thick laminated composite femoral component for hip arthroplasty. With a laminated composite stem, the designer has the freedom to vary the orientation of each ply and the stacking sequence to achieve beneficial stiffness, stress distribution, component strength, and physiological performance [3,6,17,23–26]. With this in mind, we developed our methodology for designing composite orientation and stacking sequence with the objective to maximize the composite stem fatigue strength in critical regions while minimizing stress shielding effects and keeping the interfacial stresses below user-defined maximum levels. In this paper, we present a numerical method for predicting the progressive failure of a thick laminated composite femoral component. A 3-D global/3-D local technique was developed to capture the overall structural response of this system while also enabling the 3-D ply-level stress state to be determined efficiently and accurately. Different failure criteria and material degradation models were incorporated in this method, giving it the flexibility to simulate a wide range of materials and structures. We also conducted numerical modeling to

support the design of experimental test methods for component fatigue testing, which closely simulated in vivo loading conditions. We then conducted parametric studies with the numerical model of an experimental system and compared the results to the damaged behavior of the experimentally determined composite component to assess which parameter set most accurately predicted the actual damage development behavior. Finally, we then applied the best-fitting parameter set to analyze simulated in situ composite femoral components for comparing a variety of implant designs.

## MATERIALS AND METHODS

In this paper, we present the progressive failure analysis of laminated composite femoral components for hip arthroplasty. This analysis was approached by a five-step procedure:

1. Develop and verify a 3-D FE methodology that is both efficient and accurate for the progressive failure analysis of thick composite laminates.
2. Construct an anatomical femoral model with a composite femoral prosthesis and perform a global-level analysis to predict the strain energy density (SED) distribution within the femoral component under loading conditions simulating the toe-off phase of gait.
3. Use the SED distribution from the anatomic femoral model to design an experimental test fixture to accurately simulate in vivo loading conditions and perform fatigue tests of laminated composite stems using the designed test fixture.
4. Perform progressive failure analyses of composite femoral components in the experimental test fixture and adjust the damage development model to accurately represent the experimental test data obtained in step 3.
5. Perform a progressive failure analysis of a laminated composite femoral component implanted in a human femur using the adjusted damage development model.

Each of these steps is addressed in detail in the following sections.

### Step 1: Progressive Failure Analysis Methodology

To perform the failure analysis of a laminated composite structure, we first had to predict damage initiation. Usually, damage initiation is correlated with the stress field in the structure. Although a number of methods are available that allow the contextual analysis of structural designs using composite materials, the complex and fully 3-D nature of the structural response while using composites in THA applications makes straightforward 3-D stress analysis computationally intractable [24,25]. In this research, we used a 3-D global/3-D local technique to determine the 3-D structural stress fields for thick composite laminates [23–27]. In this method, the displacements from a localized portion of a coarse global model of the entire structure were applied as boundary conditions to solve an independent highly refined model of the designated localized area of interest isolated from the structure. The key steps of applying this method are as follows:

1. An adequate global FE analysis of the entire structure is performed first.
2. The critical spot that requires further analysis is then identified from the global solution and the interpolation region is specified.
3. An adequately refined local model is developed within the global-local space.
4. The global displacements are then interpolated over the global-local space to give the boundary conditions for the local model.
5. The refined local model is then analyzed so that the 3-D stress state can be accurately determined.

The advantage of this method is that it combines the accuracy of the full 3-D solution in the area of interest with the computational efficiency provided by global/local technique. Preliminary studies have indicated that the 3-D global/3-D local technique can result in as much as 1 to 2 orders of magnitude reduction in CPU time compared with a conventional fully refined 3-D model while still maintaining a high degree of accuracy [23–27,29]. Stress analysis based on this method also has the distinct advantage that it can be used readily to locate the high-stress critical regions of the composite laminates and thus does not require a prior definition of the local model.

Once the stresses are determined, damage initiation and propagation models can be employed to predict failure processes. Element damage can be predicted with the application of an appropriate failure criterion, and one

typically can account for this by reducing the stiffness of the damaged element corresponding to the selected material degradation model. In other composite systems, predicted damage behavior has been previously shown to be quite sensitive to both the applied failure criteria and the material degradation models [30–33]. Each failure criterion applies different weighting to the effect of each stress component with respect to its respective strength parameter, while different material degradation models strongly influence how stress is redistributed following element damage. In this present work, we selected and incorporated several different failure criteria and material degradation models into the methodology to model a wide range of materials and structures. The damage models considered included three different failure criteria (Independent Criterion, Tsai-Wu Criterion, and Intralaminar and Interlaminar Criterion) and two different material degradation models (Total Discount Method and Limited Discount Method) [17,18,30–33].

*Independent Failure Criterion*

Mode 1 (fiber failure) is shown as

$$\left|\sigma_{11}/X\right| \geq 1 \text{or} \sigma_{13} \bullet \sigma_{13} + \sigma_{12} \bullet \sigma_{12} \geq \sigma^2_f \ , \quad (1)$$

Mode 2 (transverse cracking perpendicular to the 2 direction) as

$$\left|\sigma_{22}/Y\right| \geq 1 \text{or} \sigma_{21} \bullet \sigma_{21} + \sigma_{23} \bullet \sigma_{23} \geq \sigma^2_m \ , \quad (2)$$

Mode 3 (Transverse cracking perpendicular to the 3 direction) as

$$\left|\sigma_{33}/Z\right| \geq 1 \text{or} \sigma_{31} \bullet \sigma_{31} + \sigma_{32} \bullet \sigma_{32} \geq \sigma^2_m \ , \quad (3)$$

where $\sigma$ represents stress; subscript 1 represents the fiber direction, subscript 2 represents the direction transverse to the fiber but in the plane of the laminate, and subscript 3 represents the direction transverse to the fiber and to the laminate; $X = X_t$ if $\sigma_{11} > 0$; $X = X_c$ if $\sigma_{11} < 0$; $X_t$ and $X_c$ are the tensile and compressive strength of the lamina in the fiber direction; $Y = Y_t$ if $\sigma_{22} > 0$; $Y = Y_c$ if $\sigma_{22} < 0$; $Y_t$ and $Y_c$ are the tensile and compressive strength of the lamina in the 2 direction; $Z = Z_t$ if $\sigma_{33} > 0$; $Z = Z_c$ if $\sigma_{33} < 0$; $Z_t$ and $Z_c$ are the tensile and compressive strength of the lamina in the 3 direction; and $\sigma_f$ and $\sigma_m$ represent fiber shear and matrix shear strength, respectively [32].

*Tsai-Wu Criterion*

$$F_i\sigma_i + F_{ij}\sigma_i\sigma_j \geq 1 \ , \quad (4)$$

for $i = 1$ to 6 and $j = 1$ to 6. The terms in the criterion are defined as

$$\begin{aligned}
&\sigma_1 = \sigma_{11}, \sigma_2 = \sigma_{22}, \sigma_3 = \sigma_{33}, \sigma_4 = \sigma_{23}, \sigma_5 = \sigma_{13}, \sigma_6 = \sigma_{12},\\
&F_1 = 1/X_T - 1/X_C,\ F_2 = 1/Y_T - 1/Y_C,\ F_3 = 1/Z_T - 1/Z_C,\\
&F_{11} = 1/(X_T X_C),\ F_{22} = 1/(Y_T Y_C),\ F_{33} = 1/(Z_T Z_C),\\
&F_{44} = 1/R^2,\ F_{55} = 1/S^2,\ F_{66} = 1/T^2,\\
&F_{12} = -(X_T X_C Y_T Y_C)^{-0.5}/2,\ F_{13} = -(X_T X_C Z_T Z_C)^{-0.5}/2,\\
&F_{23} = -(Y_T Y_C Z_T Z_C)^{-0.5}/2, \qquad (5)
\end{aligned}$$

where $X$, $Y$, and $Z$ are the longitudinal strengths in the 1, 2, and 3 directions; subscripts $T$ and $C$ represent tensile and compressive quantities; and $R$, $S$, and $T$ represent shear strengths in the 23, 13, and 12 planes, respectively. The coefficients $F_1$, $F_2$, and $F_3$ correspond to the linear stress terms, and $F_{11}$, $F_{22}$, $F_{33}$, $F_{44}$, $F_{55}$, and $F_{66}$ correspond to the quadratic stress terms. $F_{12}$, $F_{13}$, and $F_{23}$ are the coefficients that consider the interaction effect of various normal stress components.

The Tsai-Wu Criterion identifies element damage, but it does not identify the damage mode. The method proposed by Reddy et al. was used to identify the damage mode [32]. With the use of this method, the damage mode is identified by the stress component that contributes the maximum amount to the failure index.

*Intralaminar and Interlaminar Criterion*

$$(\sigma_{11}^2/X_C X_T) - (\sigma_{11}\sigma_{22}/X_C X_T) + (\sigma_{22}^2/Y_T^2) + (\sigma_{12}/S)^2 \geq 1 \quad (6)$$

$$(\sigma_{33}/Z)^2 + (\sigma_{13}/S)^2 + (\sigma_{23}/S)^2 \geq 1, \quad (7)$$

where $\sigma$ represents stress; subscript 1 represents the fiber direction, subscript 2 represents the direction transverse to the fiber but in the plane of the laminate, and subscript 3 represents the direction transverse to the fiber and to the laminate; and $X$, $Y$, $Z$, and $S$ are the normal strengths of the lamina in the 1, 2, and 3 directions and the shear strength, respectively. Subscripts $C$ and $T$ represent compression and tension, respectively.

*Total Discount and Limited Discount Methods*

Two different material degradation models were implemented in this methodology. In the Total Discount Method,

the stiffnesses of the damaged element are dropped to zero, while some residual stiffnesses are maintained in the Limited Discount Method after element damage. In this research program, the degraded properties of the equivalent damaged element were set to be a constant multiple of the material properties before degradation. The constant, which is given a value between 0 and 1, is called the stiffness reduction coefficient (SRC) [32]. In the Total Discount Method, SRC = 0 while in the Limited Discount Method, $0 < SRC < 1$. The material degradation models were defined by three independent variables: SRC1, SRC2, and SRC3 as related to 3-D damage modes (fiber failure, matrix failure, and delamination, respectively). We defined each damage model by selecting the specified failure criterion and specified SCRs: SRC1, SRC2, and SRC3. The inclusion of various damage models represented quite a broad base of possible failure responses of the laminated composite structure.

Once established, the methodology was then implemented into commercial FE software ABAQUS (Hibbit, Karlsson, and Sorensen, Pawtucket, Rhode Island) [34]. ABAQUS provides an interface, whereby any mechanical constitutive property can be added to the property library; in our case, the constitutive model for the elements was programmed in a user subroutine called UMAT [34]. After implementation, this developed methodology was applied to the failure analysis of laminated composite structures with preliminary documented failure behavior to demonstrate its effectiveness. We considered several laminated composite structures to evaluate the validity of the progressive failure analysis methodology [26,27]. The numerical predictions agreed well with the literature reported results [24–27].

### Step 2: Finite Element Analysis of Femur-Implant Structure

In this research, an anatomic 3-D model of the right femur was developed from sequential transverse computerized tomography (CT)-scan sections taken every 3.0 mm along the length of an average-sized actual adult human femur. Edge contours defining the periosteal and endosteal boundaries and those delineating cortical and cancellous bone (where appropriate) were identified from each CT slice with image processing software National Institutes of Health (NIH) Image® (http://rsb.info.nih.gov/nih-image) [24]. The image analysis process used to identify boundaries was as follows:

1. A minimal set of control points was chosen interactively by the analyst and connected automatically by linear line segments to describe a perceived prototype of a boundary (periosteal or endosteal, or boundary delineating cortical and cancellous bone).
2. A large number of additional equal-spaced points were generated between each analyst-specified control point to give adequate freedom for the "best" edge to be detected.
3. A search for the best edge points was then conducted in the region centered around the generated approximate edge points.

In the solid modeling, separated splines were generated connecting each set of edge points, where each set of edge points may represent periosteal boundaries, endosteal boundaries, or transitions between cortical and cancellous bone. The 3-D geometry of the femur was then created with the use of spline curves representing each cross-section (2-D) and with the connection of the adjacent cross-sections (3-D).

In addition, once the edge contours were defined, the space identified to be cancellous bone was gridded out into many subregions. For each of these regions, the centroidal coordinates of the region and the maximum and minimum pixel density of the region were acquired with the use of a custom-written routine within the image processing software NIH Image® (http://rsb.info.nih.gov/nih-image) [24]. Areas of cortical and cancellous bone within the femur were then assigned different material properties based on their mineral densities inferred from the gray-scale intensity factor obtained from the CT-scan images. For use as a control, the average gray-scale intensity of regions known to be cortical bone (diaphysis regions) was recorded, and these regions correspond to bone apparent densities of 1.8 g/cm$^3$ [24]. The second control was the average gray-scale intensity of water, which represents zero apparent bone density. A linear interpolation between CT gray-scale numbers (Hounsfield numbers) and apparent density was performed with the use of control gray-scale intensities and the apparent densities for cortical bone and water, respectively. The maximum and minimum apparent densities for each of the gridded regions representing cancellous bone were derived based on the linear interpolation. The maximum and minimum Young's moduli for each of these regions were then computed from the following equation relating Young's moduli ($E$) of cancellous bone to apparent densities ($\rho$) [24,36,37]:

$$E = -0.29 + 4.2\rho + 1.8\rho^2 \qquad (8)$$

The maximum and minimum Young's moduli derived for each of the many regions were averaged and were then associated to the centrodial coordinates of each region such that each modulus value was associated to a particular location on or in the femur. The cortical bone was divided into metaphyseal and diaphyseal areas, which were assigned the orthotropic properties (**Table 1**) used by Cheal et al. [7]. **Figure 1(a)** shows the anatomic 3-D femur model, which was constructed using the FE modeling software I-DEAS (SDRC Inc., Milford, Ohio) [35], with each of the closed circles representing a single transverse CT-scan image (only the periosteal curves are shown in the figure). The prototype composite components were modeled as being fabricated from a carbon fiber-reinforced polyetheretherketone (C/PEEK) laminated plate, wherein a prosthesis blank was cut from a consolidated thick composite laminate and its contour was machined with CAD-CAM (computer-assisted design-computer-assisted manufacturing) machining according to the designated external geometry [19]. The C/PEEK properties are shown in **Table 2** [38]. The external geometry (**Figure 1(b)**) was selected to minimize stress concentration effects at the neck region of the prosthesis, while otherwise providing a noncemented canal-filling prosthesis sized to fit the selected femoral model. We then translated and rotated the prosthesis model as necessary to attain the appropriate position when inserted into the modeled femur. The resection and reaming operations were then performed with the femur model. The splines and curves of each bone-prosthesis section were appropriately modified to represent the cortical and cancellous bone sections to construct the femur-implant solid model.

**Table 1.**
Material properties of cortical bone.

| Cortical Bone | Elastic Modulus (GPa) | | | Shear Modulus (GPa) | | |
|---|---|---|---|---|---|---|
| | $E_a$ | $E_b$ | $E_c$ | $G_{ab}$ | $G_{ac}$ | $G_{bc}$ |
| Diaphysis | 21.9 | 14.6 | 11.6 | 6.99 | 6.29 | 5.29 |
| Metaphysis | 17.5 | 11.7 | 9.3 | 5.59 | 5.03 | 4.23 |

Note: *a*-axis corresponds to long axis of bone, *b*-axis corresponds to circumferential direction, and *c*-axis corresponds to radial direction. Poisson's Ratio: $\nu_{ab}$ = 0.205, $\nu_{ac}$ = 0.109, and $\nu_{bc}$ = 0.302.

The solid model was meshed with high-order 3-D elements (element types C3D20 and C3D15 in ABAQUS). Regions containing cortical and cancellous bone were assigned orthotropic and heterogeneous isotropic moduli, respectively, as discussed previously. At the global level, the femoral component was modeled with the use of 3-D elements, where each element incorporated several composite plies within it. Each layer of elements thus represented a sublaminate in which the smeared element stiffness properties [24–27] (based on the long-wave approach [39]) were set to be equivalent to the set

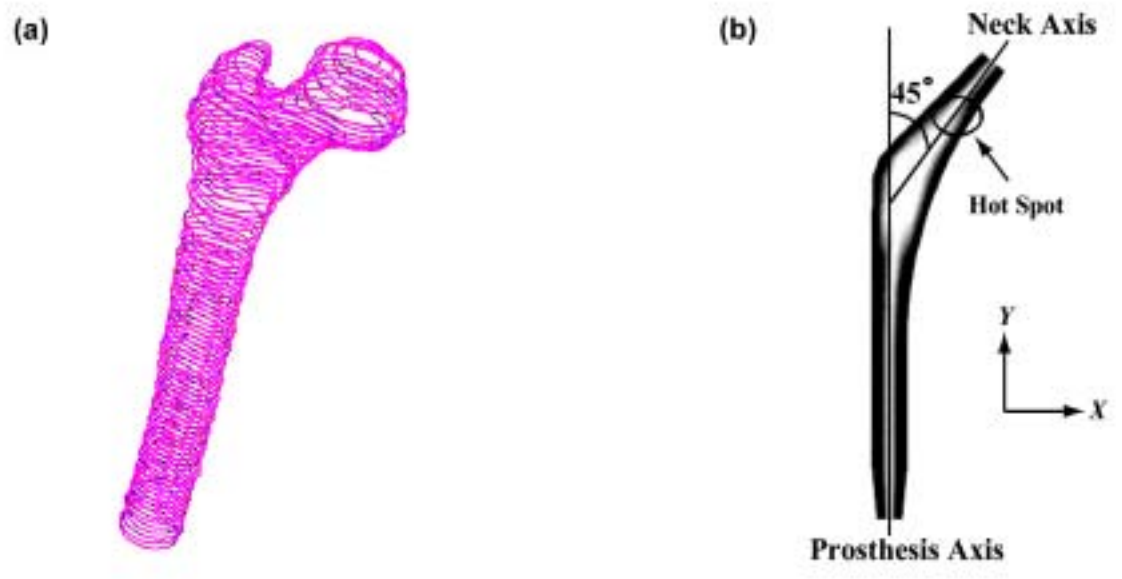


**Figure 1.**
**(a)** Solid model of proximal femur and **(b)** composite hip prosthesis with coordinate axis and geometry defined.

**Table 2.**
Material properties of C/PEEK unidirectional composite prepreg (APC-2/AS4).

| Mechanical Parameters | Values |
|---|---|
| In-plane longitudinal modulus | $E_{XX}$ = 135.3 GPa |
| In-plane transverse modulus | $E_{YY}$ = 9.0 GPa |
| Out-of-plane modulus | $E_{ZZ}$ = 9.0 GPa |
| In-plane shear modulus | $G_{XY}$ = 5.2 GPa |
| Out-of-plane shear modulus | $G_{XZ}$ = 5.2 GPa |
| Out-of-plane shear modulus | $G_{YZ}$ = 1.9 GPa |
| Poisson's Ratio | $\nu_{XY}$ = $\nu_{XZ}$ = 0.34<br>$\nu_{YZ}$ = 0.46 |
| Longitudinal strength | $X_T$ = 2068 MPa<br>$X_C$ = 1448 MPa |
| Transverse strength | $Y_T$ = 86 MPa<br>$Y_C$ = 250 MPa |
| Peel strength | $Z_T$ = 86 MPa<br>$Z_C$ = 250 MPa |
| In-plane shear strength | $S$ = 188 MPa |

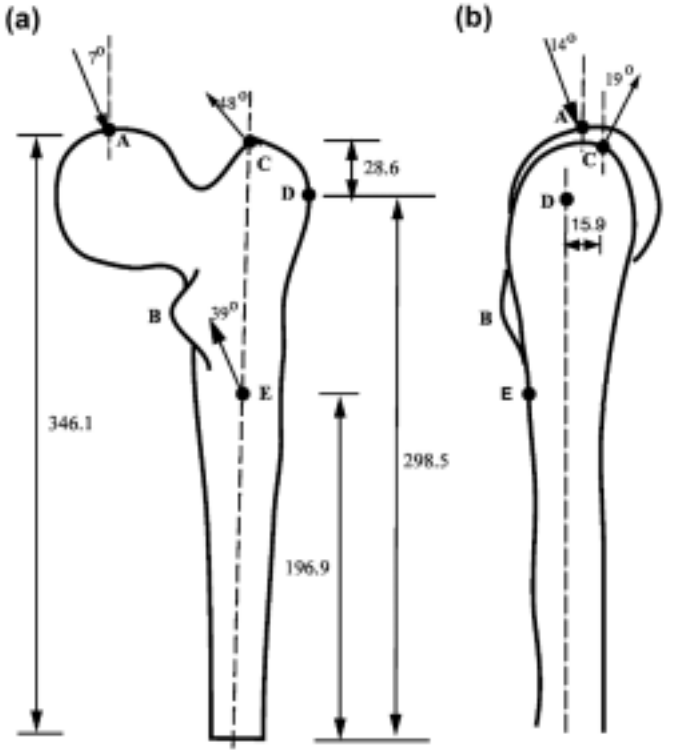


**Figure 2.**
**(a)** Posterior and **(b)** lateral views. Point of action and direction of hip joint and muscle force vectors for toe-off case (right femur, length unit: mm). A = joint contact, B = lesser trochanter, C = abductor muscle (gluteus minimus), D = abductor muscle (gluteus medius), and E = adductor muscles (superior fibers of adductor magnus).

of plies within it. This resulted in modeling efficiency by reducing the number of global elements required to capture the global structural response.

Past research has shown that mechanical loading of the joint can be reasonably accurately represented with the application of muscle and joint forces related to the designated gait activity being addressed [1]. The loading for the toe-off phase of gait was selected for simulation in this study. **Figure 2** shows the hip joint and the involved muscle forces (adductors and abductors) for the toe-off condition [7,40,41]. In **Figure 2**, hip joint, adductor muscle, and abductor muscle forces are 4.9 body weight (BW), 0.60 BW, and 1.79 BW, respectively. Body weight is assumed to be about 750 N for the present analysis [7]. The interface between the femur and the implant was represented as being fully bonded, and the femur was fully constrained distally [1]. No gap and no slippage were assumed between the prosthesis stem and the bone.

An adequate global FE analysis of the femur-implant model was then performed at this point to provide the structural responses for the design of an experimental test fixture to represent the in vivo loading conditions experienced by a composite femoral component, which is addressed later in step 3. Different criteria may be considered to represent the structural responses (strain, stress and displacement, etc.) and to specify the critical areas in the structure that required detailed analysis. The critical locations (the so-called "hot spots") and the specified interface between global and local regions (G/L interface) are usually defined by the use of contour plots of analyst-selected response measure of the global model analysis. The candidate measure of criticality can be (1) any of the six components of stresses, (2) any of the six components of strains, or (3) a combination of stresses and/or strains (stress intensity factor [SIF], strain energy release rate G, SED, or a failure criterion) [24,30]. Many different criteria are available to define failure of materials [30].

For isotropic materials, the most commonly used criteria are the maximum stress or maximum strain failure criteria. Because of the anisotropy of the material properties of composite structure, the failure criteria must be calculated usually with consideration of their ply orientations. Such information is not available in the global-level analysis.

The SED (strain energy per unit volume) represents the area under the stress-strain curve, which is a combined criterion including stress and strain components. The SED parameter has been found to correctly predict sites where potential failure of composite hip prosthesis may occur in hip arthroplasty during different activities (stair climbing, heel-strike, mid-stance, toe off, etc.) [5,17,24]. The use of SED as the hot-spot indicator also correctly predicted the area where ply-level damage initiated in the experimental studies [14,19–21,26]. Therefore, the SED distribution was selected as the critical structural response parameter for this research. It is worth pointing out that the critical areas may vary if a different critical structural response measure were used. The analyst may choose alternative hot spots for additional detailed analysis.

### Step 3: Experiment System Design and Test Method

Based on previous research, a test fixture was designed for testing composite femoral components [6,13,14,19]. Detailed dimensions of the fixture were produced with I-DEAS software to create a 3-D FE model (fixture-stem structure) for parametric studies. Several test fixture parameters were considered for the design process, including the fixture wall, potting materials, stem-potting material interface, stem support, and stem-head loading directions (**Figure 3**). The resultant load vector (stem-head loading) was applied to the center portion of the stem at the femoral head. We determined the final design from parametric studies using an FE analysis to provide a SED distribution at the critical region of the stem that best matched the femur-implant model under toe-off loading conditions.

In the experimental fixture design, a dense polymer resin plastic with elastic modulus $E$ = 3.5 GPa (CARO-PLASTIC, Carolina Biological Supply Inc., Burlington, North Carolina) was selected as the potting medium (**Figure 3**). This foundation medium was found to be able to support the high load levels required for low-cycle fatigue testing of these components [19]. We compared end-supported (i.e., an end plate supported the stem tip within the fixture) versus end-unsupported conditions (i.e., the distal tip of the stem was free to displace downward) and fully bonded versus frictionless interfaces (i.e., stem and/or foundation interface was bonded or had a gap) using FE analysis to determine the effects of these different experimental testing conditions upon the SED within the stem [26]. FE analysis showed that almost no difference existed in SED distributions in the hot spot area of the implant with these four different stem

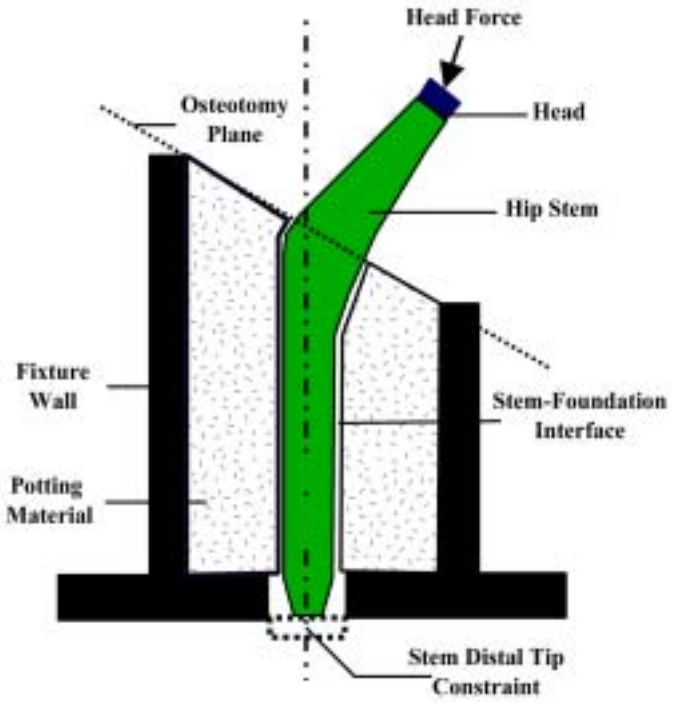


**Figure 3.**
Schematic of test fixture with hip stem.

support conditions [26]. Therefore, stem support conditions were selected that were most easily accomplished experimentally and that were most readily maintained during testing [19].

The distal tip of the stem was supported to prevent significant axial ($y$-axis) displacement of the stem within the fixture during testing, which, if not prevented, would shift the critical region away from the area of interest [19]. For the fatigue test, a nonbonded stem and/or foundation interface was selected. We also found that incorporating small flat metal plates bordering the anterior and posterior sides of the stem was necessary to prevent large torsional rotation of the implant during loading. This effect not only restrained torsional rotation of the stem but also prevented the foundation material from being overly plastically deformed during testing.

Following the completion of the fixture design, the next step was to design laminated composite femoral stems for fatigue tests. Two different stems were designed to have the same overall global structural stiffnesses but with different internal ply orientations and stacking sequences [19,23,26]. This design enabled the in situ global femur-implant model to represent both stems while providing ply-level differences, which should

influence the actual stem damage behavior. The ply stacking sequences of the Design I and II stems (in the following analysis) are shown in the following lay-ups with the angles referenced to the coordinate system shown in **Figure 1(b)**:

I: $[\pm45/\pm60/\pm30/\pm60/(\pm20)_2/\pm70/\pm5/\pm60/\pm5/\pm60/\pm25/\pm45/\pm60/\pm35/(\pm15)_2/\pm75/\pm30/\pm15/\pm25/\pm60/\pm55/\pm45/\pm20/\pm65]$ s

II: $[(\pm45)_2/(\pm60/0_2)_{10}/(\pm45)_2/\pm60/\pm35]$s

Tests of these two stems were conducted on an Instron servohydraulic 50 Kip Testing Machine [19–21]. Static tests were conducted under displacement control at a constant displacement rate of 1.0 mm/min. Fatigue load levels were conducted at 90, 80, and 70 percent of the average static damage initiation load (–11.8 kN) for the two types of stems [19]. The fatigue tests were conducted at an *R*-value of 10 and a frequency of 3 Hz. We conducted tests at three cycles per second to expedite testing, although the in vivo frequency will be generally less than one cycle per second. However, this frequency will have little effect on the fatigue response because heating caused by friction at damaged regions and hysteresis only becomes significant above five cycles per second [14,19]. The *R*-value is the ratio of the minimum force (on an absolute scale, this force represents the highest, that is, most negative, compressive force) to the maximum force (lowest, that is, least negative, compressive force) applied during fatigue loading. The specimen was cycled until an excessive amount of damage was experienced (100,000 cycles) [19]. Damage development was examined and recorded by direct stereomicroscopy and X-ray radiography methods. These test results provided information about the experimental stem behavior during progressive failure.

### Step 4: Progressive Analysis of Fixture-Stem System

In this step, we identified the critical region of the femoral component using SED as the performance criterion based on the global-level FE solution of the fixture-stem structure. Once located, the local domain was discretized with high-order 3-D elements, where one element was used per ply in the thickness direction. Previous studies have shown that this meshing level provides reasonably accurate through-the-thickness stresses [24,32]. We then performed analysis with the detailed local model to provide the ply-level stress states and damage development behavior.

We conducted parametric studies with different damage models on local models of the fixture-stem structure to evaluate how a specific damage model parameter set influenced the predicted ply-level damage development behavior in the stems. The parameters that were considered included the three different failure criteria and the two different material degradation models as discussed in step 1. We compared the predicted results with different parameters to the experimental behavior of the composite hip stems in terms of the damage mode, location, and relative severity to identify the one set of damage model parameters that most closely simulated the actual damage observed. This process thus represents an adjustment of the damage model to the actual structural performance of laminated femoral components.

### Step 5: Progressive Failure Analysis of Femur-Implant Model

Based on the global-level solutions of the femur-implant model in step 2, the critical region was identified with the use of SED as the criterion. After isolating the critical region, we created a refined 3-D local model in the specified local zone and discretized it using 20-node brick elements or 15-node wedge elements, where one brick element or wedge element was used per ply in the thickness direction. We then applied the adjusted parameter set that was obtained in step 4 to this present local model to predict damage behavior for the femur-implant model. Thus, the damage behavior of the two femoral component designs, representing two ply orientations and stacking sequences, were assessed for a laminated composite femoral component under loading conditions simulating the toe-off phase of gait.

## RESULTS AND DISCUSSION

### Finite Element Analysis of Femur-Implant Structure

**Figure 4** shows the femur-implant structure deformations under the toe-off loading condition. The structure was observed to deform in all three spatial directions: axial compression, bending in the A-P and M-L planes, and twisting in the horizontal plane [26]. The FE analysis also showed that the hot spot in the composite hip implant was in the anterior-medial neck region of the implant. The concentrated stresses exhibited in the anterior-medial area of the neck of the stem were approximately 30 mm distal to the proximal tip of the stem along the neck axis. These results agree well with the results from similar studies reported in the literature [5,13,14,17–21,23–25].

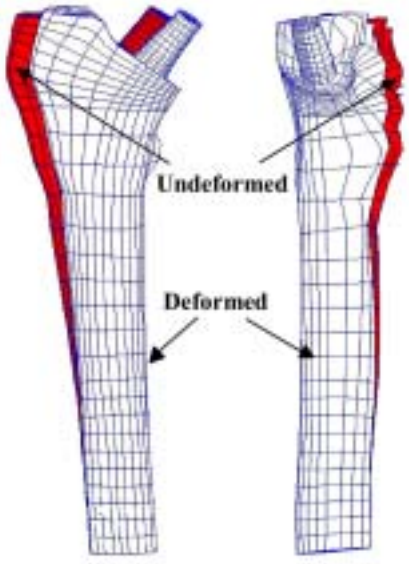


**Figure 4.**
Deformed and undeformed plot of femur-implant structure.

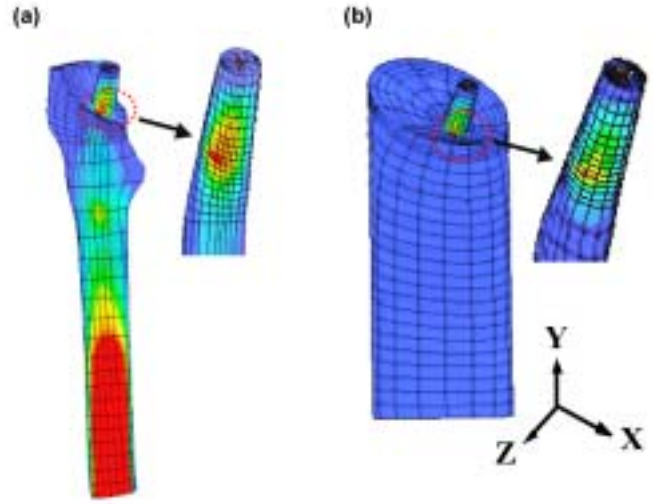


**Figure 5.**
SED distributions in **(a)** femur-implant and **(b)** fixture-stem models.

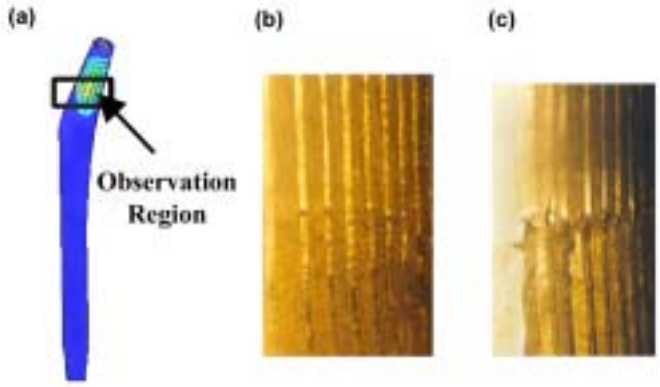


**Figure 6.**
Failures of **(a)** composite, **(b)** Design I, and **(c)** Design II stems in experimental fatigue tests.

## Experiment System Design and Test Methods

As shown by a comparison between the SED distributions in **Figure 5**, we determined an optimal fixture design from the overall test fixture design parametric studies to provide a SED distribution at the hot spot of the stem that closely matched the SED of the stem in the femur-implant model. The angles of the head force (**Figure 3**) were found to be $\theta_x$ = 85.4°, $\theta_y$ = 15.1°, and $\theta_z$ = 75.6°. The parameters, $\theta_x$, $\theta_y$, and $\theta_z$ are the angles between the head load vector and the coordinate *x*-, *y*-, and *z*-axes, respectively, using the coordinate system defined in **Figure 1(b)**.

From the experimental results, the damage in the Design I stem was found to initiate at an earlier stage as compared to the Design II, but to propagate more slowly across the primary load-bearing plies. The damage in Design I was concentrated mainly in the anterior-medial neck region of the stem. Little change and/or growth of this damage was found as fatigue loading continued, and only very localized delamination on the anterior-medial surface developed by the end of the fatigue test (100,000 cycles) (**Figure 6**). Unlike the damage in Design I, the damage in the Design II propagated rapidly. Although damage was concentrated initially on the anterior neck surface, it quickly grew transversely across adjacent plies and toward the medial side of the laminate. Matrix cracking was followed by fiber microbuckling, secondary cracking, and localized delaminations. Microbuckling occurred initially in the primary load-bearing plies across the entire anterior surface at the boundary interface of the stem-potting material (**Figure 6**). Evidently, the Design I stem was stronger and out-performed the Design II stem in the experimental fatigue tests.

## Progressive Failure Analysis of Fixture-Stem System

We performed progressive failure analysis on the detailed local model of the fixture-stem structure. The global-level to local-level model development of the fixture-stem structure is shown in **Figure 7**. We compared the numerical predictions of the ply-level damage states for each of the various sets of failure criterion and material degradation model parameters to the fatigue test

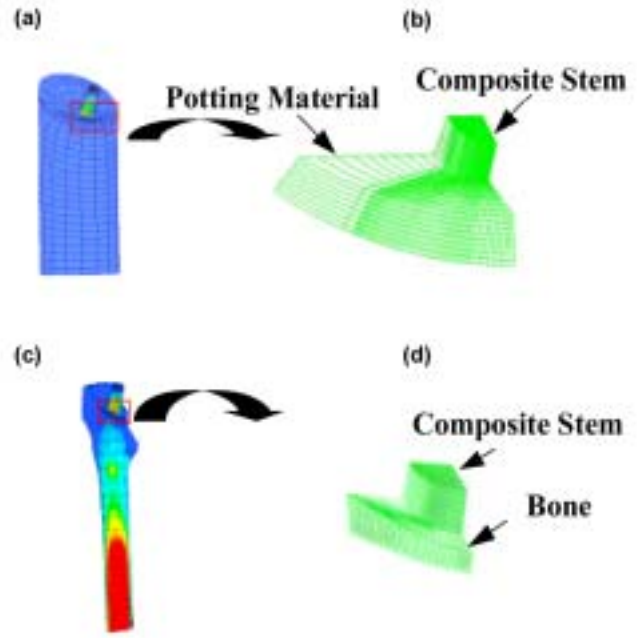


**Figure 7.**
Global and local models of **(a)** and **(b)** fixture-stem and **(c)** and **(d)** femur-implant systems.

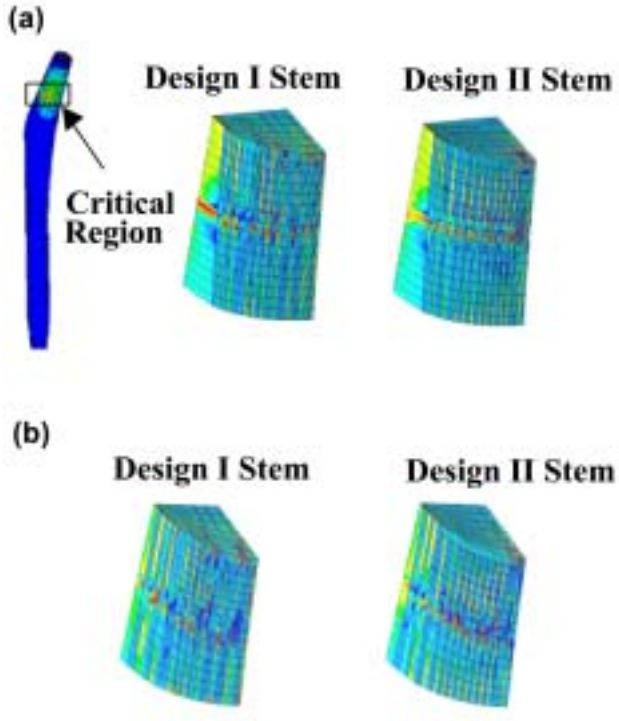


**Figure 8.**
Numerical predictions of fiber failure in stems in **(a)** fixture-stem and **(b)** femur-implant models.

results to calibrate the numerical damage model. From the comparison, the numerical predictions were determined to best match the experimental results using the Independent Failure Criterion with SRC1 = 0.01, SRC2 = 0.01, and SRC3 = 0.01 [26]. This parameter set was therefore used in the progressive failure analysis.

In the fixture-stem local model, damage in both the Design I and Design II stems was predicted to occur at the anterior-medial side of the stem, the same location that was observed experimentally. The different stacking sequences for Design I and II stems, however, provided distinctly different damage initiation and propagation behavior (**Figure 8**).

Initial fiber damage for Design I was predicted in the +30° ply (per the global coordinate system as shown in **Figure 1**) on the outside of the anterior neck surface. This corresponds to –31° with respect to a local coordinate system with 0° defined by a vector parallel to the free edge of the ply pointing toward the femoral head. Although fiber damage continued to occur at other plies moving toward the center of the laminate, the damage continued to grow in the form of local delamination and matrix damage along the axis of the applied load. The damage seemed to be constrained to the plies that had experienced initiation at low load levels (**Figure 8**). The fiber damage for Design II was predicted initially in the two +60° plies on the outside of the anterior surface. This corresponds to –1° with respect to a local coordinate system, with 0° again defined by a vector parallel to the free edge of the ply pointing toward the femoral head.

The next +60° plies moving toward the center of the laminate also had fiber damage. More damage locations were found throughout this design, because of the high number of +60° plies. Unlike damage in the Design I stem, damage in the Design II stem was predicted to propagate from the ±60° plies to other adjacent ±0° and ±45° plies. Damage was evident across the entire thickness of the laminate in the local model, from the anterior surface to the center of the laminate in Design II stem (**Figure 8**). In comparison to Design II, evidently, Design I initiated damage at a slightly lower load level than Design II. Although Design I restrained damage growth better than Design II, damage in Design II was more catastrophic during damage propagation. In other words, Design I exhibited damage propagation controlled fatigue life while the fatigue life of Damage II was initiation controlled. Based on the analysis, Design I should be more fatigue resistant than Design II. This result agreed quite well with the experimental observations [19].

### Progressive Failure Analysis of In Situ Composite Femoral Components

Progressive failure analysis was also performed on the detailed local model of the femur-implant structure. The global-level to local-level model development of the femur-implant structure is shown in **Figure 7**. The damage model parameter set identified from the previous section was then applied for the progressive failure analysis of the femur-implant model. **Figure 8** shows the damage development of the implant in the two different designs in the simulated femur-implant structure. The prosthesis was predicted to fail at the neck for the two designs. For both Design I and Design II, fiber failure was predicted to occur over the critical spots. The compressive stresses along the fiber direction $\sigma_{11}$ in the hot spots were predicted to reach their longitude compressive strength (–1448 MPa). At positions 10 mm above or below the hot spots, no fiber damage was predicted to occur. Ply damage in Design II was shown to be more concentrated and continuous over the critical zone cross section of the stem, thus unloading the volume of material above and below the damaged area. The more widely dispersed damage in Design I indicates the capability of the damaged plies to continue to transfer load across the critical zone cross section of the stem, thus showing a greater degree of structural integrity.

The responses of the stems with the fixture-stem (**Figures 6 and 8**) and femur-implant structures (**Figure 8**) are quite similar in terms of damage initiation and propagation, as expected, although the foundation conditions were different. However, damage initiation and propagation occurred differently between the two different stem designs. These results indicate that the ply orientation and stacking sequence have important effects on the structural damage behavior as anticipated. In the femur-implant structure, the Design I stem was also shown to be able to better restrain damage growth compared to the Design II stem, which exhibited a catastrophic level of damage propagation. Therefore, Design I is predicted to be more damage resistant than Design II.

### Further Considerations for Composite Femoral Component Design

In the paper, we have shown that the stress state in the femoral neck is the critical area regarding stem fatigue behavior. Based on St. Venant's principle [42], the mechanism of stem support at the implant-bone interface should not significantly alter the stress state in the femoral neck. This was found to be true in the FE analysis of the experimental conditions with the stem in the potting material with different modes of fixation (e.g., with or without distal stem support, fully fixed interface or frictionless interface). In our models, the interface between the femur and the implant was therefore represented as being fully bonded for simplicity, although this is well recognized as representing an extreme over simplification of the conditions of the actual stem-bone interface. Although the state of the bone-prosthesis interface was found not to significantly affect the results of the analysis on the fatigue strength of the composite stem in the femoral neck region, it is important to point out that bone-prosthesis interface conditions can be expected to be more severe in a compliant implant system compared to a more rigid stem and should be recognized as being quite important for composite implant design.

As discussed in the Introduction section, the stem-bone interface is an area of stress concentration with much higher stresses than for a more rigid metallic implant. This is inherent in the capability of a compliant stem to transfer load to the bone more proximally to reduce stress-shielding effects. If load is transferred to the femur more proximally, it must involve higher interfacial stresses to accomplish the more rapid load transfer via the interface. Likewise, the composite stem will also tend to result in greater motion at the bone-implant interface than with current high-modulus metal stems if the interface becomes unbonded. For example, under the various joint-loading simulations applied, our compliant composite stem design was found to undergo maximum displacements that were about 30 percent higher than a similar-shaped titanium alloy stem [24]. Larger relative micromotions at the bone-prosthesis interface may cause the formation of an unstable fibrous tissue layer and lead to implant failure. In addition, polymeric composite materials may be more vulnerable to wear than metals because of their much lower wear resistance. Designers must therefore consider the concerns associated with wear debris generation when loosening occurs and the inflammatory responses that the wear debris subsequently may induce.

While novel prostheses using composite structure with graded mechanical properties may achieve a more suitable pattern of interfacial stresses and highly relieve these interface stress concentrations [6], clearly, the treatment of the interface problem is a critical issue. Solving this problem requires further study and analysis and is beyond the scope of this current research. However, we would like to emphasize that bone-prosthesis interface

problems can be expected to be just as challenging as the stem fatigue problem, if not more so, and must also be solved before composite stems should ever be considered for actual clinical use.

## CONCLUSION

By adequately adjusting test parameters of the experimental system, we closely matched the SED distributions in the critical regions of the composite femoral components between the fixture-stem and femur-implant structure. This global critical response match provides the basis for comparing the structural responses of the composite stem designs. In this paper, we modified the potting regions and the loading directions compared to the ISO (Organization for Standardization) 7206 standard for the fatigue testing of hip prosthesis. The composite prosthesis was supported and loaded by a parametrically designed fixture to attain the stress distributions in the implant that most closely matched the simulated in vivo implanted femur model. Tests with this modified fixture are expected to be more realistic than those tests with the ISO 7206 system. This fixture design allowed damage development to be monitored in the two different stem designs in the fatigue tests. By adjusting predicted damage development with different damage models, we obtained excellent agreement between predicted and actual damage development within the composite femoral components using the Independent Failure Criterion with SRCs of SRC1 = 0.01, SRC2 = 0.01 and SRC3 = 0.01. This parameter set was then used for the progressive failure analysis of both fixture-stem and femur-implant structures.

A 3-D FE analysis has been developed for analyzing progressive failure of composite hip prosthesis implanted in an anatomical femur model. Using this methodology, we were able to simulate the effect of the ply orientation and stacking sequence of the composite femoral components on the response of prosthesis-femur system. Two different implant designs were compared in terms of their strength. For the hip prosthesis stems described here, the failure was predicted to occur at the anterior-medial neck region of the implant. This is consistent with the experiments we performed and with the results reported in the literature. Based on the analyses and the experiments, improved damage resistant was shown that it could be generated in composite implants. However, one must exercise caution regarding the results of the numerical analysis. Different loading conditions and implant shapes may affect the results of the critical regions and the optimal designs.

Results showed that the internal design characteristics (i.e., ply orientation and stacking sequence) have very important effects on the structural damage behavior of composite femoral components. This implies that a laminated composite femoral component should be able to be designed with improved damage resistance by changing laminate ply orientation and stacking sequence. The developed methodology was suitable for locating the critical region within the composite femoral component, providing 3-D ply-level stress distributions and predicting damage initiation and propagation efficiently and accurately. This research thus provides a method for effectively evaluating the damage response of the implant as a function of the ply-level design parameters. This research may lead to the use of the analytical and numerical models as initial design tools for THA before extensive experimental tests are conducted for the design of damage resistant composite structures for implant applications. Furthermore, the methods developed in this study are not specific for femoral component design, but are readily applicable to other applications, which involve using structural composite materials for implant design.

## ACKNOWLEDGMENTS

We thank Dr. Sundar Srinivasan, Dr. Wei Fu, Dr. Dan Warner, and Dr. Tom Eason for their valuable discussions and suggestions.

## REFERENCES

1. Cristofolini L. A critical analysis of stress shielding evaluation of hip prostheses. Crit Rev Biomed Eng 1997; 25(4,5):409–83.
2. Harris WH. The first 32 years of total hip arthroplasty: one surgeon’s perspective. Clin Orthop Rel Res 1992; 274:6–11.
3. Huiskes R, Weinans H, van Rietbergen B. The relationship between stress shielding and bone resorption around total hip stems and the effects of flexible materials. Clin Orthop Rel Res 1992;274:124–34.
4. Koeneman JB, Overland MK, Longo JA. Design, analysis, and material considerations of a composite material

artificial hip implant. In: Wise DL, Trantolo DJ, Altobelli DE, Yaszemski MJ, Gresser JD, Schwartz ER, editors. Encyclopedic handbook of biomaterials and bioengineering. Part B: Vol. 1. New York: Marcel Dekker, Inc.; 1995. p. 171–87.

5. Allcock S, Ali MA. Early failure of a carbon-fiber composite femoral component. J Arthroplasty 1997;12(3): 356–58.
6. Evans SL, Gregson PJ. Composite technology in load-bearing orthopaedic implants. Biomaterials 1998;19: 1329–42.
7. Cheal EJ, Spector M, Hayes WC. Role of loads and prosthesis material properties on the mechanics of the proximal femur after total hip arthroplasty. J Orthop Res 1992; 10(3):405–22.
8. Sumner DR, Turner TM, Igloria R, Urban RM, Galante JO. Functional adaptation and ingrowth of bone vary as a function of hip implant stiffness. J Biomech 1998;31: 909–17.
9. Barrack RL. Economics of revision total hip arthroplasty. Clin Orthop Rel Res 1995;319:209–14.
10. Turner TM, Sumner DR, Urban RM, Galante JO. Maintenance of proximal cortical bone with use of a less stiff femoral component in hemiarthroplasty of the hip without cement. J Bone Joint Surg Am 1997;79A:1381–90.
11. Magee FP, Weinstein AM, Longo JA, Koeneman JB, Yapp RA. A canine composite femoral stem—an in vivo study. Clin Orthop Rel Res 1988;235:237–52.
12. McKellop H, Ebramzadeh E, Saramiento A, Niederer P. Comparison of the stability of press-fit hip prosthesis femoral stems using a synthetic model femur. J Orthop Res 1991;9:297–305.
13. Liao K, Reifsnider KL. A life prediction model for fatigue loaded composite femoral prosthesis. In: Jamison RD, Gilbertson LN, editors. Composite materials for implant applications in the human body: characterization and testing. ASTM STP 1178. Philadelphia (PA); 1993. p. 72–85.
14. Liao K, Lee SS, Reifsnider KL. Compression response of a fatigue-loaded composite hip prosthesis. In: Groves SE, Highsmith AL, editors. Compression response of composite structures. ASTM STP 1185. Philadelphia (PA); 1994. p. 243–57.
15. Akay M, Aslan N. Numerical and experimental stress analysis of polymeric composite hip joint prosthesis. J Biomed Mater Res 1996;31:167–82.
16. Kaddick C, Stur S, Hipp E. Mechanical simulation of composite hip stems. Med Eng Phys 1997;19(5):431–39.
17. Yildiz H, Ha S, Chang FK. Composite hip prosthesis design. I. Analysis. J Biomed Mater Res 1998;39:92–101.
18. Yildiz H, Ha S, Chang FK. Composite hip prosthesis design. II. Simulation. J Biomed Mater Res 1998;39:102–19.
19. Granger C. Fatigue behavior of flexible-stemmed carbon/PEEK femoral components for total hip arthroplasty [MS thesis], Clemson (SC): Clemson University; 2000.
20. Li C, Granger C, Schutte HD, Biggers SB, Latour RA, Kennedy JM. Fatigue characterization of a composite femoral component for hip arthroplasty. Part I: Test fixture development. J Compos Mater. In press 2003.
21. Li C, Granger C, Schutte HD, Biggers SB, Latour RA, Kennedy JM. Fatigue characterization of a composite femoral component for hip arthroplasty. Part II: Fatigue behavior evaluation. J Compos Mater. In press 2003.
22. Humphrey SM, Gilbertson LN. Fatigue testing of femoral hip prostheses with a two beam simulated femoral bone support fixture. In: Jamison RD, Gilbertson LN, editors. Composite materials for implant applications in the human body: characterization and testing. ASTM STP 1178. Philadelphia (PA); 1993. p. 27–40.
23. Fu W. Design optimization of a laminated composite femoral component for total hip joint arthroplasty [thesis]. Clemson (SC): Clemson University; 1998.
24. Srinivasan S. 3-dimensional stress analysis of in situ FRP composite femoral components for total hip arthroplasty [thesis]. Clemson (SC): Clemson University; 1996.
25. Srinivasan S, Biggers SB, Latour RA. Analysis of composite structures using the 3-D global/local method. J Reinforced Plast Compos 1997;16(4):353–71.
26. Li C. Progressive failure analysis of laminated composite femoral prostheses for total hip arthroplasty [thesis]. Clemson (SC): Clemson University; 2000.
27. Li C, Granger C, Schutte H, Biggers SB, Kennedy JM, Latour RL. Progressive failure analysis of thick composite laminates using 3-D Global/3-D Local method. J Compos Mater. In press 2003.
28. Huiskes R, Verdonschot N. Biomechanics of artificial joints: The hip. In: Mow VC, Hayes WC, editors. Basic Orthop Biomech. Philadelphia: Lippincott Williams & Wilkins; 1997. p. 395–460.
29. Whitcomb JD. Iterative global/local finite element analysis. Comput Struct 1991;40(4):1027–31.
30. Soden PD, Hinton MJ, Kaddour AS. A comparison of the predictive capabilities of current failure theories for composite laminates. Compos Sci Technol 1998;58:1225–54.
31. Tan SC. Stress concentrations in laminated composites. Lancaster (PA): Technomic; 1994. p. 345–91.
32. Reddy YSN, Moorthy CMD, Reddy JN. Non-linear progressive failure analysis of laminated composite plates. Int J Nonlinear Mech 1995;30(5):629–49.
33. Sleight DW. Progressive failure analysis methodology for laminated composite structures. NASA/TP-1999-209107; 1999.
34. ABAQUS users manual. Version 5.8. Pawtuket (RI): Hibbit, Karlsson, and Sorensen, Inc.; 1998.

35. I-DEAS solid modeling user's guide. Master series. Milford (OH): SDRC Inc.; 1994.
36. Rho JY, Ashman RB, Turner CH. Young's modulus of trabecular and cortical bone material: ultrasonic and microtensile measurements. J Biomech 1993;26(2):111–19.
37. Carter DR, Hayes WC. Compressive behavior of bone as a two-phase porous structure. J Bone Joint Surg Am 1977; 59-A:954–62.
38. Thermoplastic Composite Material Handbook. Laguna Hills (CA): ICI Composites Inc.; 1992.
39. Sun CT, Li S. Three dimensional effective elastic constants for thick laminates. J Compos Mater 1988;22:629–39.
40. Brattain MA. Hip joint simulator design [MS thesis]. Clemson (SC): Clemson University; 1998.
41. Latour RA, Brattain MA. Femoral strain profiles under simulated 3-D muscle and joint loads for heel strike, midstance, and toe off. Crit Rev Biomed Eng 2000;28(1,2): 109–13.
42. Timoshenko SP, Goodier JN. Theory of elasticity. New York: McGraw-Hill; 1987. p. 39–40.

Submitted for publication June 18, 2001. Accepted in revised form December 9, 2002.